ACS APPLIED MATERIALS & INTERFACES

www.acsami.org

Research Article

Probing Viscoelastic Properties and Interfaces in High-Density Polyethylene Vitrimers at the Nanoscale Using Dynamic Mode Atomic Force Microscopy

Lanti Yang,* Pierre Nickmilder, Henk Verhoogt, Theo Hoeks, and Philippe Leclère*

Cite This: *ACS Appl. Mater. Interfaces* 2024, 16, 38501−38510

Read Online

ACCESS | Metrics & More | Article Recommendations

ABSTRACT: Vitrimers are a new class of heterogeneous polymers that combine the best features of thermosets with those of thermoplastics. The introduction of cross-links strongly changes the viscoelastic behavior of vitrimer materials. However, the characterization and understanding of the nanostructures and interfaces in vitrimers resulting from dynamic cross-linking formation remain a major challenge. Here, using dynamic modes of atomic force microscopy (AFM), namely intermodulation AFM (ImAFM) and AFM-based dynamic mechanical analysis (AFM-nDMA), local viscoelastic properties and interfaces at the nanoscale length of high-density polyethylene (HDPE) vitrimer materials are reported. ImAFM imaging in combination with the *k*-means clustering algorithm clearly reveals two distinct phases in the vitrimer system with highly different viscoelastic properties. AFM-nDMA further provides quantitative nanoviscoelastic properties at the nanoscale to confirm that there is a cross-linking-rich aggregation area forming a nanosize network structure in the cross-linking-poor matrix phase. The cross-linking-rich region shows a similar elastic modulus but much higher adhesion force measured by AFM compared to the cross-linking-poor HDPE matrix. Furthermore, the frequency influence on the local viscoelastic properties of HDPE vitrimer at the nanoscale was initially screened. The observed HDPE vitrimer nanostructures and viscoelastic properties at the nanoscale also provide explanations on the observed bulk HDPE vitrimer crystallinity decrease and dimensional stability increase compared to HDPE. Therefore, probing the viscoelastic properties and interfaces of HDPE vitrimer provides important insights into understanding of the correlations between the vitrimer nanostructure and the bulk mechanical and rheological behaviors.

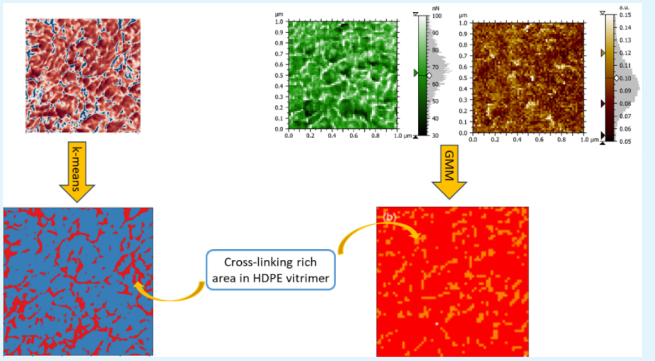

KEYWORDS: *AFM-nDMA, ImAFM, HDPE vitrimer, viscoelasticity, cross-links, interface*

Downloaded via SABIC GLOBAL TECHNOLOGIES BV on August 6, 2024 at 07:09:51 (UTC).
See https://pubs.acs.org/sharingguidelines for options on how to legitimately share published articles.

INTRODUCTION

Heterogeneous polymer materials such as polymer blends or polymer nanocomposites provide attractive material design and application opportunities compared to single-component polymer systems.[1−3] The microstructure, morphology, and interface formation in heterogeneous polymer materials have a significant influence on the material's bulk mechanical properties.[4−7] Among different heterogeneous polymer materials, in the early 2010s, Leibler and coworkers introduced the term "vitrimers" for a new class of polymers that combine the best features of thermosets with those of thermoplastics.[8] The presence of dynamic exchangeable cross-links enables the vitrimers to change their topology: at elevated temperatures, rapid exchange reactions occur, allowing vitrimers to exhibit fluidic behavior like viscoelastic liquids; at low temperatures, exchange reactions are slow and the vitrimers behave like thermosets.[8,9] In this way, vitrimers possess the enhanced mechanical and chemical resistance of cross-linked polymers at temperatures (thermoset-like) and the ability to be reprocessed, recycled, and welded at elevated temperatures (thermoplastic-like). The concept of vitrimers was first demonstrated in an epoxy network using the well-known transesterification reaction.[8] Since then, various types of exchange reactions such as transcarbonation,[10] transalkylation,[11] olefin metathesis,[12] dioxaborolane metathesis,[13] boronic ester transesterification,[14] vinylogous transamination,[15] disulfide metathesis,[16−18] etc. have been applied to various thermoset materials to form vitrimers.

Numerous investigations on turning commercial PE into PE vitrimers have been conducted to further improve the impact

Received: April 25, 2024
Revised: June 17, 2024
Accepted: June 28, 2024
Published: July 12, 2024

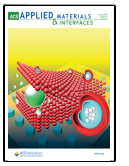

ACS Publications

© 2024 American Chemical Society

strength, dimensional stability at high temperatures, and the creep resistance of commodity polyethylene (PE). During these studies, PE vitrimers were produced via different chemical approaches to generate dynamic cross-links in PE either by reactive extrusion[13,19−21] or by reactive blending.[22] Among various studies, disulfide metathesis has been shown to be a catalyst-free exchange reaction by multiple studies in the literature.[16−18,23,24] More recently, Montoya-Ospina et al.[25] also described the formation of LLDPE (linear low density polyethylene) vitrimers containing disulfide exchange bonds via reactive extrusion of maleic anhydride-functionalized LLDPE with dithiodianiline.

It has been shown in several papers[20,21,25,26] that the incorporation of cross-links significantly alters the viscoelastic behavior of the thermoplastic matrix, leading to the rheological performance resembling that of cross-linked rubbers. This phenomenon is highly probable to be attributed to the distinctive viscoelastic properties exhibited by the formed cross-linked clusters or aggregates in contrast to the thermoplastic matrix. Ricarte et al.[26,27] described that a two-phase morphology was formed, consisting of cross-linked aggregates in a PE matrix. Based on the synchrotron-sourced small-angle X-ray scattering (SAXS) analysis, they proposed a schematic of two-phase PE vitrimer morphology characterized by a cross-link-rich network domain featuring a typical nanometer scale width dispersed within a cross-linking-poor matrix. Despite the numerous papers presented in the literature, the question remains how the introduction of (dynamic) cross-links influences the nanostructure of PE vitrimers due to the lack of nanoscale high-resolution images for interface visualizations and the deficiency of measurements capable of mapping the local microphase and interface properties in PE vitrimers.

Therefore, it is of great interest to provide more morphology and property information on the nanostructure of vitrimers which can contribute to a better understanding of the bulk mechanical and rheological behavior. Due to the time- and frequency-dependent features of the vitrimer materials, the detection and mapping of local viscoelasticity in PE vitrimers at rheologically relevant frequencies, ranging from 0.1 to 200 Hz, are very promising to help provide better understanding of the vitrimer nanostructure, the cross-linking dispersion, and interfaces. Recently, different dynamic atomic force microscopy (AFM) modes such as intermodulation AFM (ImAFM)[28] and AFM-based dynamic mechanical analysis (AFM-nDMA)[29,30] have been developed. Dynamic mode AFM enables the characterization of tip and sample surface interactions across various velocities (frequencies), allowing for the identification of microphases and interfaces with different nanoscale viscoelastic properties.[29−32]

For ImAFM, the cantilever is oscillated at two frequencies in proximity to the resonance frequency. The nonlinear nature of the tip−surface interaction leads to frequency mixing, also known as intermodulation.[32] A multifrequency lock-in technique is employed to measure numerous high-order intermodulation products, providing complex details regarding the tip−surface interaction.[33,34] This multifrequency response spectrum can directly illustrate how elastic (conservative) and viscous (dissipative) forces between the tip and the surface depend on the amplitude of cantilever oscillation. The intermodulation spectrum contains ample information to distinguish significant variations in surface viscoelastic properties from different scanned areas.[31,35] Moreover, diverse clustering algorithms are incorporated into the mode to categorize pixels into different clusters, aiming to group pixels with similar mechanical properties together into one cluster.[36] Recent studies have demonstrated that ImAFM can emphasize phases with distinct viscoelastic properties and exhibit the advantage of differentiating microphases or interfaces in complex multiphase polymer blends.[31]

AFM-nDMA is an AFM-based approach designed for dynamic mechanical analysis (DMA) through the application of modulation force to the tip−sample interaction.[37−39] Similar to bulk DMA, the AFM-nDMA measurements enable the quantitative measurements of polymer viscoelasticity such as storage modulus (E'), loss modulus (E''), and damping factor ($\tan \delta$) at the nanoscale. This method also allows one to determine the viscoelastic behaviors at a fixed position of the sample surface at multiple frequencies within the rheologically relevant frequency range for polymers.[29] With sub-100 nm resolution, AFM-nDMA is very promising to elucidate the local structural changes and the formation of interphases.[29,40−42] Very recently, Nguyen et al.[43] has reported a direct mapping of dynamic mechanical responses at the interface of a model epoxy nanocomposite under the transition from a glassy to a rubbery state using an AFM-based nDMA technique. They found an enhanced viscoelastic response at the interface compared to the bulk matrix in the glass state, offering insights into the nanoscale toughening mechanism in epoxy nanocomposites.

In this study, both ImAFM and AFM-nDMA are applied for the first time to explore the nanostructure and interfaces of high-density polyethylene (HDPE) vitrimer by characterizing the local viscoelastic properties. The findings not only provide deeper insight into the dynamic cross-link dispersion in the HDPE vitrimer material but also reveal the local viscoelastic property differences at the cross-linking-rich area and HDPE-rich area. The information obtained from the nanostructure and interface of vitrimer also helps in elucidating the thermal behavior and bulk mechanical properties of the HDPE vitrimer material.

MATERIALS AND METHODS

Materials (Sample Information). Utilizing the same chemical methodology as Montoya-Ospina et al.[25] developed, SABIC's HDPE 0863F (MFI = 8 g/10 min (190 C/2.16 kg)) was functionalized with maleic anhydride (MAH) via reactive extrusion by employing a proprietary, in-house developed method. The amount of MAH grafted onto the HDPE backbone was determined to be 2 wt %. Subsequently, the MAH-functionalized HDPE was reacted with dithiodianiline (DTA) (purchased from Sigma-Aldrich) via reactive extrusion in a Xplore micro compounding unit (MCU). Cryo-milled MAH-functionalized HDPE was dry-blended with DTA, and this mixture was fed to the MCU through small steps to control the applied force. Reactive extrusion was conducted at 210 °C, with a screw speed of 100 rpm and a reaction time of 5 min. The resultant HDPE vitrimers were compression molded into plaques (100 × 100 × 1 mm) or discs (diameter of 25 mm and thickness of 1 mm) in a Fontijne Press at 175 °C.

Sample Preparation for AFM Analysis. Both the HDPE and HDPE vitrimer materials were selected for dynamic mode AFM analysis. The prepared cross-section of the samples in the flow direction of molding was cryo-microtomed at −120 °C using microtoming equipment (LEICA EM UC7) to obtain a flat cross-sectional surface. A diamond knife (Diatome) mounted on a stainless-steel holder was used for microtoming

https://doi.org/10.1021/acsami.4c06809
ACS Appl. Mater. Interfaces 2024, 16, 38501−38510

the samples. After cryo-microtoming, the microtomed blocks were directly used in AFM measurements without further treatment.

Tapping Mode AFM Imaging. AFM experiments were performed using a Dimension FastScan AFM system (Dimension FastScan, Bruker, Santa Barbara, USA). Software Nanoscope Analysis 9.4 from Bruker was used as a computer interface for operation, and Nanoscope Analysis 2.0 from Bruker was used for the analysis of AFM measurements. All AFM measurements were performed under ambient conditions. For rubber distribution characterization, the AFM tapping mode was used at a scan rate of 1 Hz utilizing tapping mode AFM tips (Model Bruker RTESPA-300, k: 42 N/m, f: 320 kHz, and r < 10 nm).

ImAFM on the HDPE Vitrimer. ImAFM analysis was performed using a Dimension Icon AFM (Bruker Corp.) coupled with an external multifrequency lock-in amplifier and software for calibration and nanomechanical analysis (Intermodulation Products AB).[28] All scans were conducted at a resolution of 512 × 512 pixels with a line rate frequency of 0.5 Hz. Tapping mode AFM silicon cantilevers (Model Bruker RTESPA-300, k: 42 N/m, f: 320 kHz, and r < 10 nm) were used for ImAFM measurements. As detailed in the Introduction, an external multifrequency lock-in amplifier was used for the ImAFM mode to excite the cantilever at two frequencies near the resonance frequency, while recording the response at 42 intermodulation products (mixing products) of the two drives.[28] The measurement was begun with a thermal noise calibration[44] of the cantilever. The calibration provided the constant required to convert the measured detector signal into nanometers of cantilever deflection. After calibration, all force and deflection data were presented in the calibrated units of nanoNewtons (nN) and nanometers (nm).[31]

Following the selection of the maximum drive amplitude for the cantilever motion in nanometers, the determination of individual drive frequencies, amplitudes, and phase shifts was carried out through an automatic methodology routine. The above-mentioned Dimension Icon AFM (Bruker Corp.), set to the contact mode, was used as the host AFM to control the scanning, while a feedback error signal was supplied by the multifrequency lock-in the amplifier. During scanning the surface, the amplitude and phase shift of the cantilever deflection at numerous frequencies were measured by the lock-in amplifier and software for each pixel in the image.[34] After imaging, the k-means clustering algorithm[36] was applied to the data set comprised of the measured quadrature response at 42 frequencies. The k-means algorithm sorted the pixels into different clusters, aiming to minimize the Euclidean distance between the pixels of the same cluster.[31] Each cluster was then characterized by the mean value of each feature in the cluster, enabling the derivation of an average elastic response curve (F_I) and viscous response curve (F_Q) for each cluster.

AFM-nDMA. AFM-nDMA was performed using a Dimension Icon AFM (Bruker Corp.). Precalibrated, high-accuracy AFM silicon cantilevers (RTESPA-300−30, k = 40 N/m, r = 30 nm, from Bruker Corp.) were used for AFM-nDMA measurements. The photodiode deflection sensitivity was determined by collecting force curves on a sapphire sample. Two types of measurements were performed: single frequency modulation mapping and multifrequency modulation sweep.

Single frequency modulation mapping was carried out at a frequency of 80 Hz (to avoid the electrical noise of the European electrical circuit for which the frequency is 50 Hz). The scans had a resolution of 64 × 64 pixels and were acquired over a squared micrometer area. The scan time was roughly 40 min.

Both single frequency and multifrequency data sets were collected with a trigger force of 25 nN and a force modulation of 10 nN. The phase lag of nanoDMA measurements was calibrated with the measurement on the rigid sapphire sample.

Multifrequency modulation sweep was executed at fixed positions. The frequency ramp for the sweep contained the frequencies of 1, 1.8, 3.2, 5.8, 10.5, 19, 40, 62, 80, 111, and 160 Hz applied in a random order to avoid dynamic effects. 80 Hz was the reference frequency which was used to estimate the contact radius during the contact process. The measurements were repeated 9 times for each frequency.

To distinguish local structures and interphase in the single frequency mapping measurement, we used homemade clustering software. By selecting relevant channels (guided with a correlation test to avoid the overlapping of data), the data were divided into an arbitrary number of clusters, based on the k-means clustering algorithm[36] or Gaussian mixture model algorithm.

Transmission Fourier-Transform Infrared (FTIR) Measurements. FTIR measurements using a previously developed method[25] were performed using a PerkinElmer Spectrum 100 FTIR to verify the cross-linking reaction occurring between the MAH group and the NH_2 group of DTA on the HDPE vitrimer cold pressed film. Each measurement consisted of 9 scans in a wavenumber range of 4400−400 cm^{-1} with a spectral resolution of 4 cm^{-1}.

HDPE Vitrimer Bulk Thermal Properties by Differential Scanning Calorimetry (DSC). The melting behavior and crystallinity of HDPE and HDPE vitrimer were determined by DSC (Q20 DSC apparatus, TA Instruments) under a nitrogen atmosphere. The samples were heated from 30 to 200 °C at a heating rate of 10 K/min. The degree of crystallinity was calculated using

$$X_c\,[\%] = \left(\frac{\Delta H_m}{\Delta H_m^0}\right) \times 100 \tag{1}$$

where X_c is the degree of crystallinity (%), ΔH_m is the measured enthalpy of melting (J/g), and ΔH_m^0 is the theoretical enthalpy of melting for 100% crystalline PE (293 J/g).

HDPE Vitrimer Bulk Dynamic Mechanical Analysis (DMA). A Q800 DMA apparatus (TA Instruments) was used to measure the mechanical properties as a function of temperature of HDPE vitrimers. Rectangular samples were used in a tensile mode to perform temperature sweep. All tests were performed at a constant frequency of 10 Hz and a constant strain of 0.1%.

The cross-linking density (ν) was calculated using the storage modulus (E') at 150 °C using

$$\nu = \frac{E'(T)}{3RT} \tag{2}$$

where R is the universal gas constant (8.3145 J mol^{-1} K^{-1}) and T is the absolute temperature in the rubbery region (423.15 K) as described in the literature.[25]

https://doi.org/10.1021/acsami.4c06809
ACS Appl. Mater. Interfaces 2024, 16, 38501−38510

RESULTS AND DISCUSSION

Tapping Mode AFM Characterization on the Morphology of HDPE and HDPE Vitrimer. Both HDPE and HDPE vitrimer samples were carefully cryo-microtomed to achieve a nanoscale flat surface. It is clear from Figure 1 that the remaining topography features reflect the variations in the material's mechanical properties. The flat surface also allows the phase images (Figure 1b,d) to provide a more accurate mapping of the mechanical properties. Tapping mode AFM images clearly demonstrate the morphology difference between HDPE and HDPE vitrimers. As shown in Figure 1a,b, the cross-sectional surface of HDPE sample shows a highly packed lamellar crystal structure. When the dynamic cross-linker was added to the HDPE material (Figure 1c,d), the highly packed lamellar crystal structure was not visible anymore. An interconnected network of a smaller phase shift (brighter phase) matrix with inclusions having a larger phase shift (darker phase) was observed. The larger phase shift corresponds to greater dissipation in the tip−surface interaction. Compared to HDPE with a highly packed lamellar crystalline structure, the AFM tapping mode images of the HDPE vitrimer material indicate a network structure appearing at the nanoscale. In the literature, evidence showed that the introduction of cross-linkers into vitrimers strongly changes the viscoelastic behavior of the thermoplastic matrix, leading to a decreased degree of crystallinity.[25] In order to provide in-depth understanding and establish correlations between the nanoviscoelastic behavior and the bulk properties, dynamic mode AFM techniques, including ImAFM and AFM-nDMA, were further applied for HDPE vitrimer material characterization. These experiments aimed to better illustrate the nanoviscoelastic properties and provide insight into the microphase and interface formation within the HDPE vitrimer material.

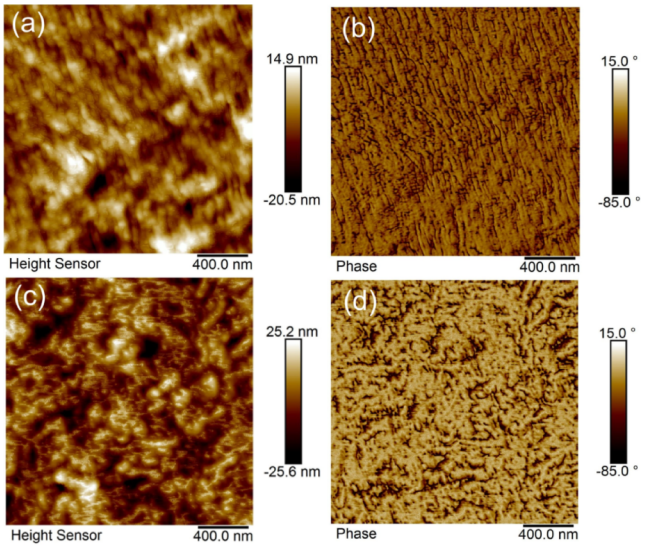

Figure 1. Tapping mode AFM height images of (a) HDPE and (c) HDPE vitrimer. Tapping mode AFM phase images of (b) HDPE and (d) HDPE vitrimer.

Probing HDPE Vitrimer Nanoviscoelastic Properties by ImAFM. The nanomechanical response of the HDPE vitrimer sample surface was studied by ImAFM. The height and phase images of the HDPE vitrimer at one of the two drive frequencies in ImAFM are shown in Figure 2. Here, the phase image (Figure 2b) clearly shows two distinct regions in the HDPE vitrimer sample with different nanomechanical responses. As mentioned in the Introduction, 42 intermodulation frequencies were applied using the ImAFM mode to understand the interaction of the various phases at different frequencies.[28] At each image pixel, an intermodulation

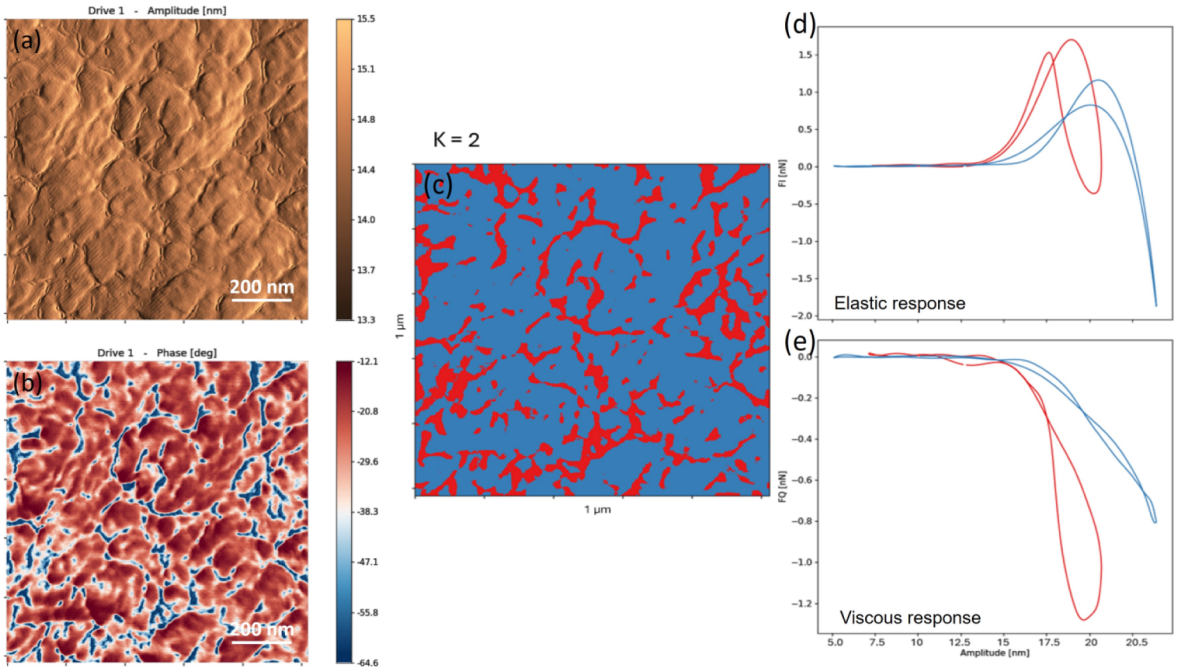

Figure 2. ImAFM height (a) and phase (b) images at the drive frequency $F1$ with a scan size of 1 μm × 1 μm. (c) Image showing pixels sorted into 2 groups using the k-means algorithm. The average elastic response curves F_I (d) and viscous response curve F_Q (e) are shown in the corresponding colors for the image pixel that was closest to the centroid of each cluster.

https://doi.org/10.1021/acsami.4c06809
ACS Appl. Mater. Interfaces 2024, 16, 38501−38510

spectrum was obtained, encompassing all the amplitudes and phase shifts of the 42 intermodulation frequencies. In order to understand better the viscoelastic response from each phase, the *k*-means clustering algorithm[36] was applied to both the amplitude and phase shift signal data set to categorize the response by grouping pixels according to their mechanical responses at each pixel from the 42 frequencies. As the phase images clearly demonstrate two distinct phases, $k = 2$ was used for the *k*-means clustering algorithm. In Figure 2c, the images of clusters using $k = 2$ are presented. It demonstrates that the two phases indeed present distinct nanoviscoelastic properties. The blue region in Figure 2d, representing the matrix, exhibits substantial repulsive forces (negative F_I) at the highest amplitudes. A lower magnitude of the dissipative force F_Q for the blue region (Figure 2e) was observed. The force quadrature curves of the blue region demonstrate significantly low hysteresis, suggesting quick recovery from deformation. Consistent with previous studies,[35] the blue region corresponds to an area with higher stiffness. Conversely, the red region is much softer, characterized by predominantly attractive force (positive F_I, Figure 2d) and a higher magnitude of dissipative force (negative F_Q, Figure 2e). The slow relaxation of this region also results in increased hysteresis, suggesting a higher content of adhesive or viscous components in the red region. Although the intermodulation spectrum generated from the tested sample area including the tapping interactions, moving surface, and AFM feedback is nonlinear and far from obvious to produce a readily interpretable map of mechanical properties,[31] the *k*-means clustering images effectively reveal the spatial clustering of domains and nanosized network structures with different viscoelastic responses in the HDPE vitrimer material. The nanosized network structure area exhibits a lower elastic modulus and higher adhesion properties when compared to the HDPE matrix phase.

Quantitative Nanoviscoelastic Property Characterization by AFM-nDMA. The AFM-nDMA technique was developed to allow accurate measurements of material's viscoelastic properties at the nanoscale.[29] More importantly, AFM-nDMA enables the measurements of the viscoelastic properties of nanosized domains within polymer blends, composites, and other heterogeneous materials with a nanoscale lateral resolution. This capability provides valuable information about nanocomponents and interfaces.[43] For our study, given that the ImAFM images have already illustrated the presence of two phases with distinct viscoelastic responses in the HDPE vitrimer sample, employing AFM-nDMA for further characterization would be highly interesting and meaningful. This approach can initially validate the findings from ImAFM regarding the vitrimer nanostructure. Additionally, nanoDMA will provide a more comprehensive understanding of the material's viscoelastic properties, including the storage modulus (E'), the loss modulus (E''), and the damping factor (tan δ), thereby providing deeper insights into the nanostructures of HDPE vitrimer.

The typical height and nanoviscoelastic property mapping images of the HDPE vitrimer sample characterized by AFM-nDMA are presented in Figure 3. 64 × 64 resolution imaging was used due to a much longer scanning time and larger data processing amount. Although the resolution of the images is not as high as that of ImAFM because the AFM probe used for AFM-nDMA has a larger radius, there are still domains with higher tan δ and adhesion property visualization in the images.

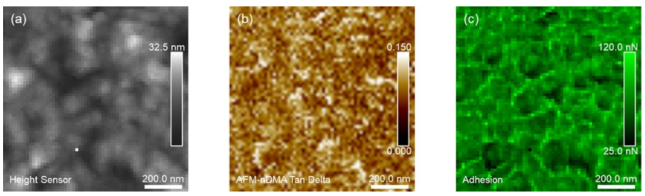

Figure 3. AFM nanoDMA: (a) height, (b) tan δ, and (c) adhesion mapping of HDPE vitrimer materials at 80 Hz with a 64 × 64 pixel resolution.

Adhesion mapping provides information on the strength of interactions between the AFM tip and the surface, revealing variations in adhesion at different locations of the scanned area. Tan δ mapping, on the other hand, provides information on the viscoelastic properties of the material, revealing variations in energy dissipation at different locations. Although both adhesion and tan δ mapping yield valuable information on the mechanical properties of the materials, the results they provide may not always be consistent. Interestingly, the domains with high tan δ are not always the same for the domains with high adhesion suggesting that there are a variety of molecular arrangements in these regions.

Similar to the *k*-means clustering applied in the ImAFM imaging, a data clustering method with first a cross-correlation analysis and then data clustering using Gaussian mixture modeling (GMM) has been developed and applied on the height channel and the other 14 nanoviscoelastic property mapping channel data in an independent and unsupervised way. A schematic drawing for demonstrating the AFM-nDMA data analysis and clustering procedures is presented in Figure 4.

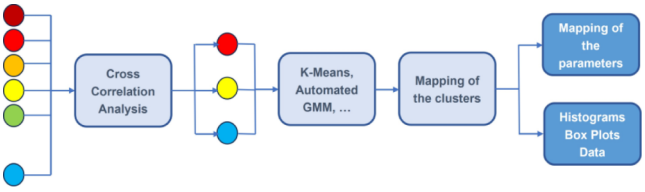

Figure 4. Schematic drawing for the data analysis and clustering procedure in AFM-nDMA data processing.

Using the AFM-nDMA data of HDPE vitrimer, the cross-correlation analysis demonstrated the most significant importance and difference from the log modulus and adhesion data channels. Therefore, AFM-nDMA data from these two channels were selected for further GMM clustering. The ImAFM *k*-means clustering clearly demonstrated two phases in the vitrimer material with different viscoelastic properties. In order to further validate the findings from ImAFM, here, three clusters were first applied to the images. The clustering image as presented in Figure 5b clearly shows two regions again, Cluster 0 (C0) and Cluster 1 (C1), while Cluster 2 only corresponds to very few outliers. It is highly interesting to note that the dispersion of the C1 region in the C0 region is very similar to what was found from ImAFM and *k*-means clustering. Again, here a nanosized network structure (C1) dispersed in the matrix (C0) in the HDPE vitrimer was found. The big advantage of AFM-nDMA is the possibility to obtain quantitative information for each region through a calibration procedure during measurements. Here, the storage modulus (E') and adhesion distribution from both C0 and C1 regions

https://doi.org/10.1021/acsami.4c06809
ACS Appl. Mater. Interfaces 2024, 16, 38501−38510

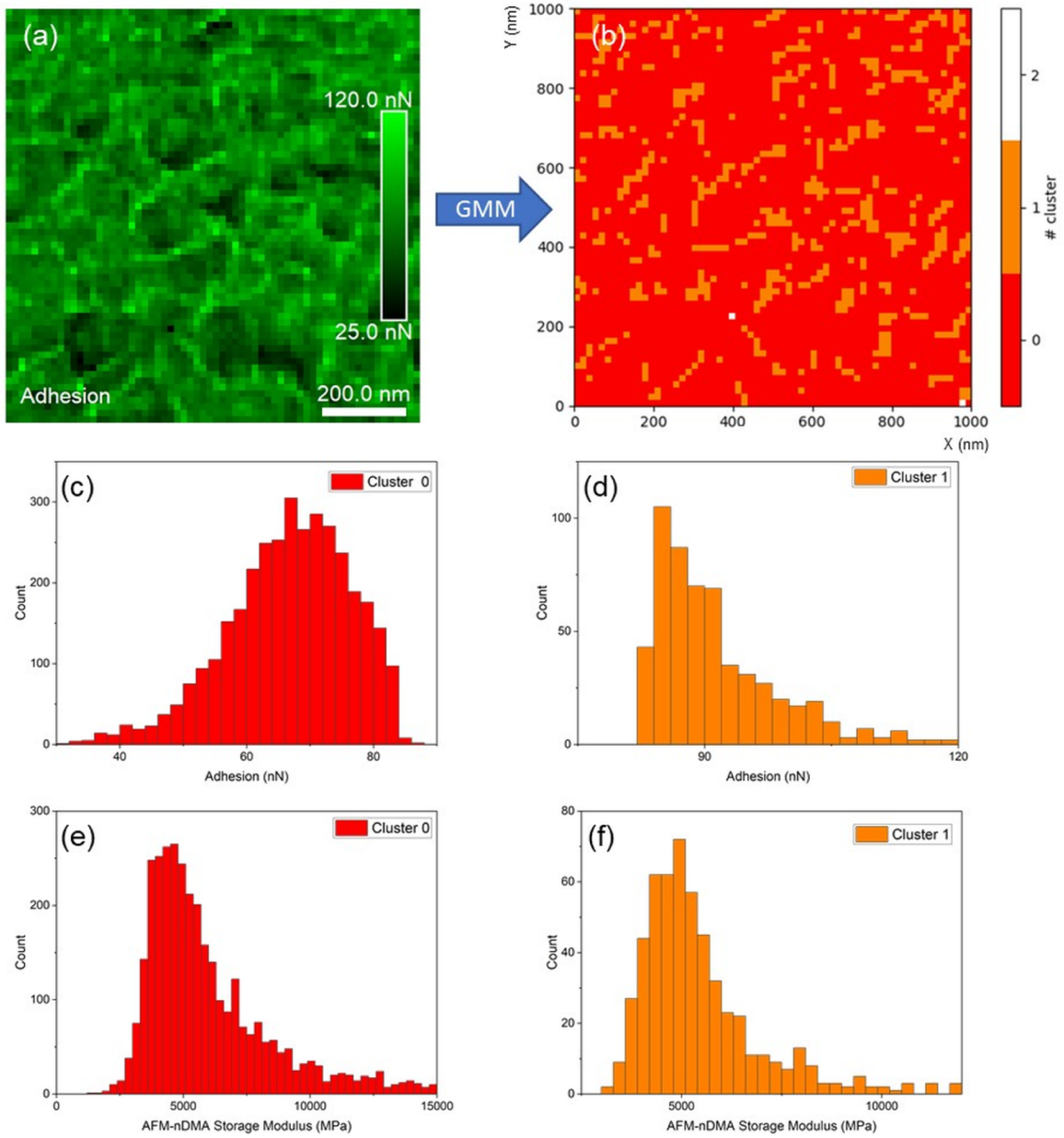

Figure 5. GMM clustering method applied to the adhesion (a) and log modulus images to obtain the three cluster (C0, C1, and C2) mapping images (b) with different adhesion or log modulus properties. The quantitative storage modulus (c) and adhesion distribution (d) for the C0 region, and the quantitative storage modulus (e) and adhesion distribution (f) for the C1 region.

are presented (Figure 5c–f). The storage modulus and adhesion distribution for both C0 and C1 regions do not follow a normal distribution. In such cases, the median values from E' and adhesion distribution provide a more representative measure to the distribution and correlate better with the peak values from the distribution. Therefore, the median values were calculated from distributions and further used for the comparison of C0 and C1 regions. The results suggest that the E' distribution of C0 matrix regions with a median storage modulus of 5.3 ± 0.1 GPa is slightly higher than the E' distribution of the C1 dispersion region (5.1 ± 0.1 GPa). A significantly larger difference is evident in the adhesion distribution between C0 and C1 regions. Notably, the median adhesion in the C1 region (89.3 ± 0.6 nN) is much higher than that of the C0 region (67 ± 0.5 nN). The quantitative nanoviscoelastic properties obtained from AFM-nDMA show similar trends compared to the qualitative nanoviscoelastic properties found from ImAFM images and *k*-means clustering. Clearly, there is a network of nanostructures (domains typically about tens of nanometer) with higher adhesion properties dispersed in the HDPE matrix phase. Recently, Tournilhac et al.[27] have performed studies to understand the phase separation and self-assembly in PE-based vitrimers. Based on the synchrotron-sourced small-angle X-ray scattering (SAXS) analysis, they proposed a schematic of two-phase PE vitrimer morphology. This schematic illustrates a cross-link-rich network domain with a typical nanometer scale width dispersed in the cross-linking poor PE domain/matrix. The proposed two-phase morphology was further supported by bulk rheology measurements.[26] Considering a similar dynamic cross-linking formation in the HDPE vitrimer materials, the morphology and nanoviscoelastic property results from both

https://doi.org/10.1021/acsami.4c06809
ACS Appl. Mater. Interfaces 2024, 16, 38501−38510

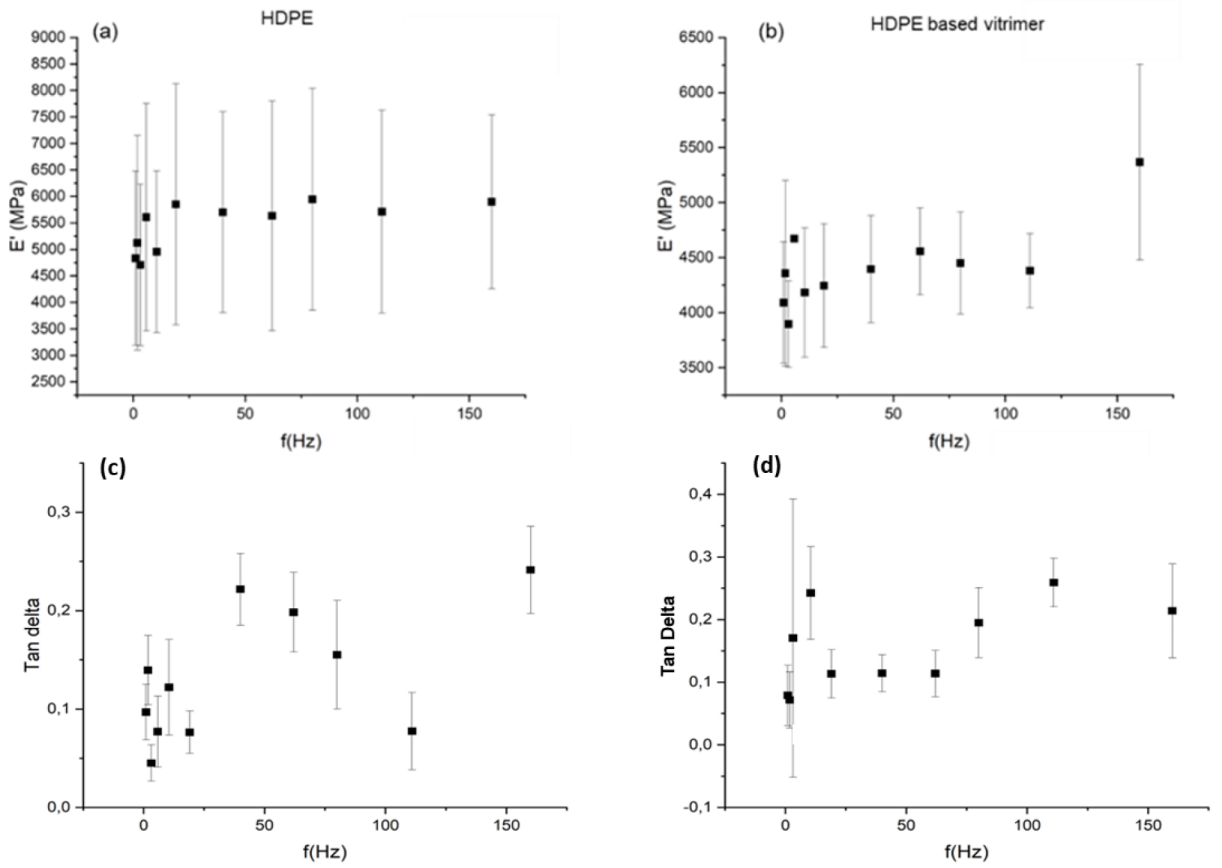

Figure 6. Storage modulus of HDPE (a) and HDPE-based vitrimer (b), and tan δ of HDPE (c) and HDPE-based vitrimer (d) at different frequencies. The values are averaged by measuring about 9 points in different regions on the sample surface for each frequency.

ImAFM and AFM-nDMA provide, for the first time, compelling evidence of the microscale two-phase morphology within the HDPE vitrimer system. Furthermore, a decreased degree of crystallinity was found in PE vitrimer compared to pure PE materials in the literature.[25,27] The slow crystallization kinetics of dynamic cross-links, leading to lower crystallinity in the graft-rich network domain, has been considered the mechanism for the crystallinity degree decrease.[27] Our FTIR spectrum of HDPE vitrimer shows a peak at 1715 cm^{-1}, which is characteristic of C═O of a maleimide ring,[25] suggesting that the cross-linking reaction between NH_2 groups of DTA and two MAH groups of the functionalized HDPE took place. It is then expected that the cross-linking-rich network domains will be probably less stiff compared to the PE-rich matrix and they show different adhesion to AFM tips due to the presence of different chemical compositions. Here, the nanosize-width network region with much stronger adhesion behavior, therefore, well demonstrates the cross-linking-rich region in the HDPE matrix.

For viscoelastic materials, the viscous response typically exhibits strong dependency on the temperature or frequency. Another advantage of AFM-nDMA is its ability to assess nanoviscoelastic properties at different frequencies or temperatures. In this study, a series of measurements were performed on both pure HDPE and HDPE vitrimer samples as a function of frequencies. Figure 6 shows the resulting curves for the storage modulus E' (Figure 6a,b) and tan δ (Figure 6c,d) at frequency sweep ranging from 0.1 to 200 Hz. Here, precalibrated AFM probes with a diameter of around 30 nm were used for the multifrequency modulation sweep executed at the fixed position. Due to the relatively larger diameter of the AFM probe used, the mechanical properties measured here predominantly reflect the average mechanical properties for the scanned area with less differentiation of different nanodomains existing in the scanned area. As shown in Figure 6a, the HDPE material shows a slightly lower storage modulus E', ranging from approximately 4.7 to 5.0 GPa at a low frequency range of up to 20 Hz. Above 20 Hz to 200 Hz, the storage modulus of HDPE remains more stable in the range between 5.5 and 6.0 GPa. Compared to pure HDPE, the HDPE vitrimer shows a slightly lower storage modulus E' at the measured frequency range. From 1 to 120 Hz, the storage modulus E' of HDPE vitrimer is in the range from 4.0 to 4.7 GPa, and significantly increase to 5.3 GPa at 160 Hz. From the AFM tapping mode image, it clearly shows that the HDPE sample exhibits highly packed PE lamellar crystal structures. ImAFM and AFM-nDMA results, on the other hand, clearly demonstrate that in the HDPE vitrimer material, there is a more complex network structure which influences the crystallinity degree and consequently, the viscoelastic response of HDPE vitrimer at different frequencies compared to HDPE. These findings explain the slightly lower modulus found in HDPE vitrimer. When comparing the storage modulus obtained from AFM-nDMA mapping at 80 Hz, the storage modulus E' of HDPE vitrimer determined from the multifrequency modulation sweep shows slightly lower values. This slight variance in the absolute storage modulus value difference may result from two factors: first, a different calibration process for the two types of measurements and second, the comparatively limited data points (9 points for each fixed position measurement)

https://doi.org/10.1021/acsami.4c06809
ACS Appl. Mater. Interfaces 2024, 16, 38501−38510

obtained from multifrequency modulation sweep, thereby resulting in increased deviation.

Tan δ from the multifrequency modulation sweep measurement for both HDPE and HDPE vitrimer is also presented in Figure 6c,d. Again, tan δ of HDPE and HDPE vitrimer show a slightly different frequency dependence. For HDPE, tan δ vibrates between 0.04 and 0.25 at the measured frequency range. For the HDPE vitrimer, there is a trend of tan δ to be more stable at the measured frequency range and vibrating from 0.08 to 0.25 at the measured frequency range.

Comparison between HDPE Vitrimer Bulk Scale and Nanoscale Characterization. Both ImAFM and AFM-nDMA demonstrated a microscale two-phase morphology within the characterized HDPE vitrimer system. In order to provide insights into the understanding of the correlations between the vitrimer nanostructure and the bulk mechanical and rheological behaviors, the bulk thermal properties of HDPE and HDPE vitrimer materials were characterized by DSC and the results are summarized in Table 1. Combining

Table 1. DSC Analysis Results of HDPE and HDPE-MAH +DTA (HDPE vitrimer)

	cooling			2nd heating		
	T_{cr} (°C)		ΔH_{cr} (J/g)	T_m (°C)		ΔH_m (J/g)
sample	peak	onset		peak	onset	
HDPE 0863F	117.2	119.3	240.8	133.7	127.2	243.4 (82%)
HDPE-MAH	113.0	119.6	193.5	128.0	115.7	182.8 (62.2%)
HDPE-MAH +DTA	111.1	117.6	185.5	129.8	116.4	189.8 (64.6%)

the AFM-nDMA imaging and frequency sweep results for HDPE vitrimer, there are a few interesting findings in relation to the bulk thermal properties of HDPE vitrimer. AFM-nDMA and ImAFM imaging show that there are less highly ordered crystalline structures and formation of a network structure for HDPE vitrimer at the nanoscale. Similarly, DSC analysis results of both HDPE and HDPE vitrimer (Table 1) bulk materials evidenced clearly that the MAH groups and the formation of cross-links decrease the degree of crystallinity of the materials. The degree of crystallinity of HDPE was 82.0%, while the degree of crystallinity of HDPE vitrimer was 64.6%, corresponding to a 17.4% decrease. The crystallinity and crystalline structure organization difference also help explain the storage modulus E' decrease in the HDPE vitrimer compared to HDPE from the multifrequency modulation sweep measurement.

Bulk DMA measurements were performed to determine the bulk HDPE vitrimer mechanical properties as a function of temperature as presented in Figure 7. The nanoscale viscoelastic properties characterized by AFM-nDMA were subsequently compared to the bulk DMA results under ambient conditions. The storage modulus (E') for both HDPE and HDPE vitrimer at RT is in the range of 4−5 GPa at the nanoscale. The bulk DMA shows that the storage modulus is in the 3−4 GPa range for HDPE vitrimer at room temperature, which is in a very similar value range compared to the newly developed nanoscale analysis. The slight difference found can be explained by the factors that first, AFM-nDMA needs calibration steps which may introduce a certain degree of differences in the absolute E' values

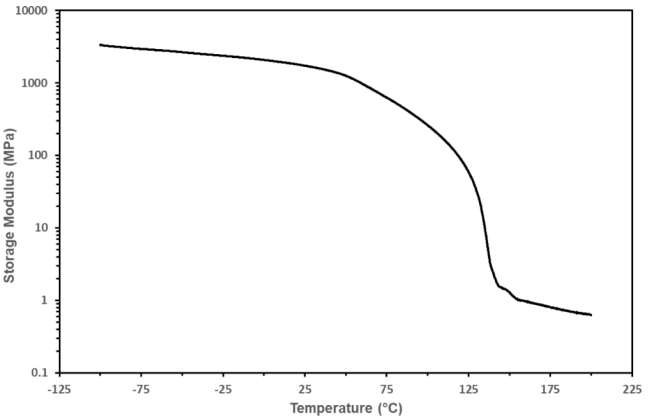

Figure 7. Dynamic mechanical analysis (DMA) on the storage modulus as a function of temperature for HDPE vitrimers (10 Hz, 0.1% strain).

compared to the bulk analysis. Second, it is important to note that AFM-nDMA uses an indentation-based stress−strain analysis approach to determine mechanical properties, whereas bulk DMA was performed using a tensile testing mode. The difference in the testing approach will result in different polymer chain orientation and deformation during testing, which potentially introduce discrepancies in the E' values.

It is well-known from the literature that a significant drop of storage modulus E' is expected for bulk PE when the material reaches its melting point, resulting in stopping the measurements.[25] Typically, above the melting temperature, the bulk PE samples flow and lead to the rupture of the sample.[45] For the HDPE vitrimer as shown in Figure 7, it is possible to retain a modulus as a rubbery plateau above the melting temperature. As mentioned in the literature, the rubbery plateau was directly proportional to the MAH and cross-linking content.[25] The cross-linking density of HDPE vitrimer was then estimated using the E' value at 150 °C to be $\sim 1.1 \pm 0.3 \times 10^{-4}$ (mol/cm^3). The cross-linking identified from bulk DMA demonstrates a strong correlation with the distinct network featuring nanodomains with higher adhesion properties in the HDPE vitrimer, as observed through both ImAFM and AFM-nDMA characterization. It is also worthy to note that the formed cross-links effectively prevented the material from fully collapsing at higher temperatures, as evidenced by the bulk DMA. This dimensional stability of HDPE vitrimer identified both at the bulk and nanoscale demonstrates well the improved processing ability at the bulk scale for HDPE vitrimer compared to conventional HDPE. Recent studies[29,43] show a strong agreement between AFM-nDMA methods and bulk mechanical testing methods for characterizing polymer mechanical properties. Our findings further endorse AFM-nDMA as a promising technique for complex multiphase polymer system characterization.

CONCLUSIONS

A novel approach using different dynamic AFM modes, namely ImAFM and AFM-nDMA, to probe the local viscoelastic properties of HDPE vitrimer materials at the nanoscale is presented in this paper. For ImAFM, a large amount of information contained in the multifrequency nonlinear response allows for comprehensive analysis and achieves the conservative and dissuasive forces with a high spatial resolution. The subsequent application of the k-means

https://doi.org/10.1021/acsami.4c06809
ACS Appl. Mater. Interfaces 2024, 16, 38501−38510

clustering method to the multiphase frequency data reveals two distinct phases in the vitrimer system, each characterized by markedly different viscoelastic properties. Based on the high-resolution ImAFM images, AFM-nDMA was applied to provide quantitative information on the viscoelastic properties of different phases in HDPE-based vitrimer. In combination with the selection of relevant channels guided with a correlation analysis and GMM clustering, the quantitative nanoviscoelastic properties obtained from AFM-nDMA not only provides clear morphological information for vitrimer materials but also suggests the presence of two distinct phases within the vitrimer system. Specifically, one phase corresponds to regions rich in cross-linking, forming a nanoscale network structure within the other cross-linking poor matrix phase. With the advanced characterization by AFM-nDMA, the storage modulus, loss modulus, adhesion, and other relevant viscoelastic property mapping of the HDPE and HDPE vitrimer in combination with viscoelastic property frequency sweep were obtained for the first time. These preliminary findings clearly show that there are differences between HDPE and HDPE vitrimer viscoelastic properties attributable to the distinct arrangements of nanostructures. This novel approach offers deeper insights into the local viscoelastic properties of HDPE vitrimer, thereby providing valuable information to establish correlations between the nanoscale cross-linking network structures and the HDPE vitrimer bulk thermal and mechanical performance.

AUTHOR INFORMATION

Corresponding Authors

Lanti Yang − *Analytical Science Europe, Corporate T&I, SABIC, Bergen op Zoom 4612 PX, The Netherlands;* orcid.org/0000-0002-5172-782X; Email: lanti.yang@sabic.com

Philippe Leclère − *Laboratory for Physics of Nanomaterials and Energy (LPNE), Research Institute in Materials Science and Engineering, University of Mons (UMONS), Mons B-7000, Belgium;* orcid.org/0000-0002-5490-0608; Email: philippe.leclere@umons.ac.be

Authors

Pierre Nickmilder − *Laboratory for Physics of Nanomaterials and Energy (LPNE), Research Institute in Materials Science and Engineering, University of Mons (UMONS), Mons B-7000, Belgium*

Henk Verhoogt − *High Performance Materials, Corporate T&I, SABIC, Geleen 6167 RD, The Netherlands*

Theo Hoeks − *Corporate T&I, SABIC, Bergen op Zoom 4612 PX, The Netherlands*

Complete contact information is available at: https://pubs.acs.org/10.1021/acsami.4c06809

Notes

The authors declare no competing financial interest.

ACKNOWLEDGMENTS

The authors gratefully acknowledge David Zoller and Jessica Jarman for reviewing the manuscript, and SABIC for the financial support. Funding source: this project was funded by SABIC.

REFERENCES

(1) Schadler, L. S.; Brinson, L. C.; Sawyer, W. G. Polymer nanocomposites: A small part of the story. *JOM* **2007**, *59*, 53−60.

(2) Fang, M.; Zhang, Z.; Li, J.; Zhang, H.; Lu, H.; Yang, Y. Constructing hierarchically structured interphases for strong and tough epoxy nanocomposites by amine-rich graphene surfaces. *J. Mater. Chem.* **2010**, *20*, 9635−9643.

(3) Shahbikian, S.; Carreau, P. J.; Heuzey, M.-C.; Ellul, M. D.; Cheng, J.; Shirodkar, P.; Nadella, H. P. Morphology development of EPDM/PP uncross-linked/dynamically cross-linked blends. *Polym. Eng. Sci.* **2012**, *52*, 309−322.

(4) Pukánszky, B. Interfaces and interphases in multicomponent materials: past, present, future. *Eur. Polym. J.* **2005**, *41*, 645−662.

(5) Mirzazadeh, H.; Katbab, A. A. PP/EPDM-based thermoplastic dynamic vulcanizates with organoclay: morphology, mechanical and viscoelastic properties. *Polym. Adv. Technol.* **2006**, *17*, 975−980.

(6) Karger-Kocsis, J.; Mahmood, H.; Pegoretti, A. Recent advances in fiber/matrix interphase engineering for polymer composites. *Prog. Mater. Sci.* **2015**, *73*, 1−43.

(7) Forrest, J. A.; Dalnoki-Veress, K.; Dutcher, J. R. Interface and chain confinement effects on the glass transition temperature of thin polymer films. *Phys. Rev. E* **1997**, *56*, 5705−5716.

(8) Montarnal, D.; Capelot, M.; Tournilhac, F.; Leibler, L. Silica-Like Malleable Materials from Permanent Organic Networks. *Science* **2011**, *334*, 965−968.

(9) Zee, N. J. V.; Nicolaÿ, R. Vitrimers: Permanently crosslinked polymers with dynamic network topology. *Prog. Polym. Sci.* **2020**, *104*, 101233.

(10) Snyder, R. L.; Fortman, D. J.; Hoe, G. X. D.; Hillmyer, M. A. H.; Dichtel, W. R. Reprocessable Acid-Degradable Polycarbonate Vitrimers. *Macromolecules* **2018**, *51* (2), 389−397.

(11) Obadia, M. M.; Mudraboyina, B. P.; Serghei, A.; Montarnal, D.; Drockenmuller, E. Reprocessing and Recycling of Highly Cross-Linked Ion-Conducting Networks through Transalkylation Exchanges of C−N Bonds. *J. Am. Chem. Soc.* **2015**, *137*, 6078−6083.

(12) Lu, Y.-X.; Tournilhac, F.; Leibler, L.; Guan, Z. Making Insoluble Polymer Networks Malleable via Olefin Metathesis. *J. Am. Chem. Soc.* **2012**, *134*, 8424−8427.

(13) Röttger, M.; Domenech, T.; van der Weegen, R.; Breuillac, A.; Nicolaÿ, R.; Leibler, L. High-performance vitrimers from commodity thermoplastics through dioxaborolane metathesis. *Science* **2017**, *356* (6333), 62−65.

(14) Cromwell, O. R.; Chung, J.; Guan, Z. Malleable and Self-Healing Covalent Polymer Networks through Tunable Dynamic Boronic Ester Bonds. *J. Am. Chem. Soc.* **2015**, *137* (20), 6492−6495.

(15) Denissen, W.; Rivero, G.; Nicolaÿ, R.; Leibler, L.; Winne, J. M.; Prez, F. E. D. Vinylogous Urethane Vitrimers. *Adv. Funct. Mater.* **2015**, *25* (16), 2451−2457.

(16) Michal, B. T.; Jaye, C. A.; Spencer, E. J.; Rowan, S. J. Inherently Photohealable and Thermal Shape-Memory Polydisulfide Networks. *ACS Macro Lett.* **2013**, *2* (8), 694−699.

(17) Imbernon, L.; Oikonomou, E. K.; Norvez, S.; Leibler, L. Chemically crosslinked yet reprocessable epoxidized natural rubber via thermo-activated disulfide. *Polym. Chem.* **2015**, *6*, 4271−4278.

(18) de Luzuriaga, A. R.; Martin, R.; Markaide, N.; Rekondo, A.; Cabañero, G.; Rodríguez, J.; Odriozola, I. Epoxy resin with exchangeable disulfide crosslinks to obtain reprocessable, repairable and recyclable fiber-reinforced thermoset composites. *Mater. Horiz.* **2016**, *3*, 241−247.

(19) Caffya, F.; Nicolaÿ, R. Transformation of polyethylene into a vitrimer by nitroxide radical coupling of a bis-dioxaborolane. *Polym. Chem.* **2019**, *10*, 3107−3115.

(20) Tellers, J.; Pinalli, R.; Soliman, M.; Vachon, J.; Dalcanale, E. Reprocessable vinylogous urethane cross-linked polyethylene via reactive extrusion. *Polym. Chem.* **2019**, *10*, 5534−5542.

(21) Zych, A.; Pinalli, R.; Soliman, M.; Vachon, J.; Dalcanale, E. Polyethylene vitrimers via silyl ether exchange reaction. *Polymer* **2020**, *199*, 122567.

(22) Ji, F.; Liu, X.; Lin, C.; Zhou, Y.; Dong, L.; Xu, S.; Sheng, D.; Yang, Y. Reprocessable and Recyclable Crosslinked Polyethylene with Triple Shape Memory Effect. *Macromol. Mater. Eng.* **1719**, *304* (3), 1800528.
(23) Zheng, X.; Yang, H.; Sun, Y.; Zhang, Y.; Guo, Y. A molecular dynamics simulation on self-healing behavior based on disulfide bond exchange reactions. *Polymer* **2021**, *212*, 123111.
(24) Si, H.; Zhou, L.; Wu, Y.; Song, L.; Kang, M.; Zhao, X.; Chen, M. Rapidly reprocessable, degradable epoxy vitrimer and recyclable carbon fiber reinforced thermoset composites relied on high contents of exchangeable aromatic disulfide crosslinks. *Composites, Part B* **2020**, *199*, 108278.
(25) Montoya-Ospina, M. C.; Verhoogt, H.; Osswald, T. A. Processing and rheological behavior of cross-linked polyethylene containing disulfide bonds. *SPE Polym.* **2022**, *3*, 25−40.
(26) Ricarte, R. G.; Tournilhac, F.; Cloître, M.; Leibler, L. Linear Viscoelasticity and Flow of Self-Assembled Vitrimers: The Case of a Polyethylene/Dioxaborolane System. *Macromolecules* **2020**, *53*, 1852−1866.
(27) Ricarte, R. G.; Tournilhac, F.; Leibler, L. Phase Separation and Self-Assembly in Vitrimers: Hierarchical Morphology of Molten and Semicrystalline Polyethylene/Dioxaborolane Maleimide Systems. *Macromolecules* **2019**, *52*, 432−443.
(28) Platz, D.; Tholén, E. A.; Pesen, D.; Haviland, D. B. Intermodulation atomic force microscopy. *Appl. Phys. Lett.* **2008**, *92* (15), 153106.
(29) Pittenger, B.; Osechinskiy, S.; Yablon, D.; Mueller, T. Nanoscale DMA with the Atomic Force Microscope: A New Method for Measuring Viscoelastic Properties of Nanostructured Polymer Materials. *JOM* **2019**, *71*, 3390−3398.
(30) Kolluru, P. V.; Eaton, M. D.; Collinson, D. W.; Cheng, X.; Delgado, D. E.; Shull, K. R.; Brinson, L. C. AFM-based Dynamic Scanning Indentation (DSI) Method for Fast, High-resolution Spatial Mapping of Local Viscoelastic Properties in Soft Materials. *Macromolecules* **2018**, *51*, 8964−8978.
(31) Kassa, H. G.; Stuyver, J.; Bons, A.-J.; Haviland, D. B.; Thoren, P.-A.; Borgani, R.; Forchheimer, D.; Leclère, P. Nano-mechanical properties of interphases in dynamically vulcanized thermoplastic alloy. *Polymer* **2018**, *135*, 348−354.
(32) Platz, D.; Forchheimer, D.; Tholén, E. A.; Haviland, D. B. Interpreting motion and force for narrow-band intermodulation atomic force microscopy. *Beilstein J. Nanotechnol.* **2013**, *4*, 45−56.
(33) Platz, D.; Forchheimer, D.; Tholén, E. A.; Haviland, D. B. Interaction imaging with amplitude-dependence force spectroscopy. *Nat. Commun.* **2013**, *4* (1), 1360−1369.
(34) Platz, D.; Forchheimer, D.; Tholén, E. A.; Haviland, D. B. The Role of Nonlinear Dynamics in Quantitative Atomic Force Microscopy. *Nanotechnology* **2012**, *23*, 265705.
(35) Haviland, D. B.; van Eysden, C. A.; Forchheimer, D.; Platz, D.; Kassab, H. G.; Leclère, P. Probing viscoelastic response of soft material surfaces at the nanoscale. *Soft Matter* **2016**, *12*, 619−624.
(36) Pedregosa, F.; Varoquaux, G.; Gramfort, A.; Michel, V.; Thirion, B.; Grisel, O.; Blondel, M.; Prettenhofer, P.; Weiss, R.; Dubourg, V.; Vanderplas, J.; Passos, A.; Cournapeau, D.; Brucher, M.; Perrot, M. Scikit-learn: Machine Learning in Python. *J Mach. Learn. Res.* **2011**, *12*, 2825−2830.
(37) Igarashi, T.; Fujinami, S.; Nishi, T.; Asao, N.; Nakajima, K. Nanorheological Mapping of Rubbers by Atomic Force Microscopy. *Macromolecules* **2013**, *46*, 1916−1922.
(38) Dokukin, M.; Sokolov, I. High-resolution high-speed dynamic mechanical spectroscopy of cells and other soft materials with the help of atomic force microscopy. *Sci. Rep.* **2015**, *5* (1), 12630.
(39) Dokukin, M. E.; Sokolov, I. On the Measurements of Rigidity Modulus of Soft Materials in Nanoindentation Experiments at Small Depth. *Macromolecules* **2012**, *45*, 4277−4288.
(40) Ellison, C. J.; Torkelson, J. M. The distribution of glass-transition temperatures in nanoscopically confined glass formers. *Nat. Mater.* **2003**, *2*, 695−700.
(41) Cheng, X.; Putz, K. W.; Wood, C. D.; Brinson, L. C. Characterization of local elastic modulus in confined polymer films via AFM indentation. *Macromol. Rapid Commun.* **2015**, *36*, 391−397.
(42) Riaño, L.; Belec, L.; Chailan, J.-F.; Joliff, Y. Effect of interphase region on the elastic behavior of unidirectional glass-fiber/epoxy composites. *Compos. Struct.* **2018**, *198*, 109−116.
(43) Nguyen, H. K.; Shundo, A.; Ito, M.; Pittenger, B.; Yamamoto, S.; Tanaka, K.; Nakajima, K. Insights into Mechanical Dynamics of Nanoscale Interfaces in Epoxy Composites Using Nanorheology Atomic Force Microscopy. *ACS Appl. Mater. Interfaces* **2023**, *15*, 38029−38038.
(44) Higgins, M. J.; Proksch, R.; Sader, J. E.; Polcik, M.; Mc Endoo, S.; Cleveland, J. P.; Jarvis, S. P. Noninvasive determination of optical lever sensitivity in atomic force microscopy. *Rev. Sci. Instrum.* **2006**, *77* (1), 013701.
(45) Mohagheghian, I.; McShane, G. J.; Stronge, W. J. Impact perforation of monolithic polyethylene plates: Projectile nose shape dependence. *Int. J. Impact Eng.* **2015**, *80*, 162−176.

https://doi.org/10.1021/acsami.4c06809
ACS Appl. Mater. Interfaces 2024, 16, 38501−38510